Biofabrication

International Society for Biofabrication

PAPER

Use of inkjet-printed single cells to quantify intratumoral heterogeneity

To cite this article: Woong Hee Yoon *et al* 2020 *Biofabrication* **12** 035030

IOP Publishing Biofabrication 12 (2020) 035030 https://doi.org/10.1088/1758-5090/ab9491

Biofabrication

PAPER

Use of inkjet-printed single cells to quantify intratumoral heterogeneity

RECEIVED
4 November 2019

REVISED
28 April 2020

ACCEPTED FOR PUBLICATION
19 May 2020

PUBLISHED
29 June 2020

Woong Hee Yoon[1,5], Hwa-Rim Lee[2,5], SungEun Kim[3], Eunjee Kim[3], Ja Hyeon Ku[4], Kunyoo Shin[3] and Sungjune Jung[1,2]

[1] Division of Integrative Biosciences and Biotechnology, Pohang University of Science and Technology, Pohang 37673, Republic of Korea
[2] Department of Creative IT Engineering, Pohang University of Science and Technology, Pohang 37673, Republic of Korea
[3] Department of Life Sciences, Pohang University of Science and Technology, Pohang 37673, Republic of Korea
[4] Department of Urology, Seoul National University Hospital, Seoul 03080, Republic of Korea

E-mail: sjjung@postech.ac.kr, kunyoos@postech.ac.kr and kuuro70@snu.ac.kr

Keywords: tumor heterogeneity, inkjet printing, single cell, tumor organoid, bladder tumor

Supplementary material for this article is available online

Abstract

Quantification of intratumoral heterogeneity is essential for designing effective therapeutic strategies in the age of personalized medicine. In this study, we used a piezoelectric inkjet printer to enable analysis of intratumoral heterogeneity in a bladder cancer for the first time. Patient-derived tumor organoids were dissociated into single cell suspension and used as a bioink. The individual cells were precisely allocated into a microwell plate by drop-on-demand inkjet printing without any additive or treatment, followed by culturing into organoids for further analysis. The sizes and morphologies of the organoids were observed, so as the expression of proliferation and apoptotic markers. The tumor organoids also showed heterogeneous responses against chemotherapeutic agent. Further, we quantified mRNA expression levels of representative luminal and basal genes in both type of tumor organoids. These results verify the heterogeneous expression of various genes among individual organoids. This study demonstrates that the fully automated inkjet printing technique can be used as an effective tool to sort cells for evaluating intratumoral heterogeneity.

1. Introduction

Intratumoral heterogeneity (ITH) refers to the existence of several clones of tumor cells in the same tumor tissue [1–3]. ITH impedes cancer therapy because the survival of drug-resistant subclones can cause tumor relapse. ITH may originate from genetic instability and evolutionary process that lead to diversity of cell lineages. Spatiotemporal variation among subclones found in many tissues hinders us from fully understanding tumor evolution, metastasis, and drug responses. The development of the next-generation sequencing methods have been widely applied to quantify intratumoral heterogeneity [4].

Because tumor tissues consist of subclones, tumor cells are required to be analyzed separately [5]. For this purpose, several single-cell approaches have been developed, including fluorescence-activated cell sorting (FACS) [6], microwells [7, 8], and microfluidic devices [9–11]. The goal of these techniques is to analyze the gene expression profile at the single-cell level. For FACS, tumor cells are fluorescently tagged and sorted for further application of drug test and sequencing data analysis. In microwells, single cells are trapped into tiny wells that have sizes of tens of micrometers. Although these two methods can sort single cells, statistical significance can only be obtained after analysis of hundreds to thousands of tumor cells. This sample size became available with a breakthrough in the microfluidic device-mediated droplet-barcoding technique [9]. It allows analysis of thousands of single cells by isolating them into separate droplets with reagents for subsequent analysis.

Piezoelectric inkjet printing (IJP) has several unique advantages that can be applied for tumor heterogeneity research. IJP uses piezocrystals to convert electric signals to physical forces that are used to eject picoliter droplets [12]. These dropets contain an average of 0.70 to 1.42 cells per droplet, depending on

[5] Both authors contributed equally to this work

the drop volume and the cell concentration [13]. Further, the ability to specifically isolate single cells were demonstrated with a 5 × 5 array of insect cells generated by manipulating the jet moment [14]. Another advantage is that IJP can generate precise patterns of multiple types of cells and hydrogels at high speed (10–1000 Hz) and at high resolution (⩽100 μm) [15–18]. Notably, such printing process has minimal influence on the cells because it can be performed in conventional cell culture media, without the need of any additive or treatment [19, 20]. IJP has little influence on the viability and the growth kinetics of the cells [21, 22]. These features encompass the advantages of the current single-cell isolation techniques such as culturing single cells in separate condition and high throughput potential, while avoiding detrimental influences on them.

In this respect, we used IJP to observe ITH. Single bladder-tumor cells were printed into separate wells of microwell plates, and cultured them for further analysis. Tumor cells were obtained from bladder cancer patients and maintained as organoids. We carried out the optimization of the printing parameters, such as cell concentration and jet frequencies, to maximize the proportion of drops that carried only one cell. The printed cells were delivered into ultralow adhesion treated microwell plates to induce organoid formation. The organoids exhibited different growth patterns, such as growth kinetics and morphologies. Variation was observed in proliferation marker, Ki-67, which was positively correlated with the organoid size. When treated with chemotherapeutic drug, the organoids showed heterogeneous responses with a few organoids showing resistancy. We further quantified heterogeneity on the mRNA expression levels through quantitative real-time PCR (qRT-PCR) analysis, and observed large variations in their gene expressions.

2. Materials and methods

2.1. Human bladder tumor samples

Fresh samples of human bladder tissue were obtained from Seoul National University Hospital (SNUH). The samples were initially obtained as 0.5–1 cm^3 specimens from patients undergoing transurethral resection of the bladder under a protocol approved by the SNUH Institutional Review Board. Informed consent and consent to publish were obtained from the patients. The cancer tissues were evaluated before being transported to Pohang University of Science and Technology for further analysis.

2.2. Tissue dissociation and tumor organoid culture

The tumor tissue was washed with DPBS (Gibco, NY, USA) and DMEM (Gibco) supplemented with 10% FBS (Millipore, MA, USA) and 1% penicillin/streptomycin (Gibco), then minced with blades. It was immersed in 10 ml of the DMEM, 10 mm HEPES, 10% FBS and 0.25 $mg{\cdot}ml^{-1}$ collagenase I/II (Thermo Fisher Scientific, MA, USA), then placed in an incubator for 1 h at 37 °C and 5% CO_2. The dissociated clusters were centrifuged at 1500 rpm for 5 min, resuspended in 5 ml of DMEM with 10% FBS, and passed through a 100 μm cell strainer (Corning, NY, USA). The cell clusters were spun down and resuspended in 200 μl of Matrigel (Corning), and plated at the center of a well of 6-well plate (Corning) to form a shape of the drop. The drop was solidified by incubation for 15 min at 37 °C and 5% CO_2. After solid drops were formed, 3 ml of organoid culture medium was added to the well, and the medium was changed every 2–3 d. For the organoid culture medium, advanced DMEM (Gibco) was supplemented with 10 mM HEPES (Sigma-Aldrich, MO, USA), 10 mM Nicotinamide (Sigma-Aldrich), 1 mM N-acetyl-L-cystein (Sigma-Aldrich), 1 μM A83-01 (Sigma-Aldrich), 10 μM Y-27 632 (Abmole, TX, USA), 50 $ng{\cdot}ml^{-1}$ epidermal growth factor, 1X GlutaMAX (Gibco), 1X B-27 (Gibco), and 1% penicillin/streptomycin.

For passaging, tumor cells were embedded in growth-factor-reduced Matrigel (Corning) at a density of 5×10^5 $cells{\cdot}ml^{-1}$. The 40 μl of the cell-laden Matrigel was located at the center of the well of a 24-well plate to form a hemisphere. The plate was flipped upside down and placed in an incubator at 37 °C and 5% CO_2 for 15 min to allow solidification. The tumor organoids were filled with 2 ml of culture medium, and the medium was changed every 2 d.

Tumor organoid formation began as early as day 2. They were passaged after 8–10 d before the average size exceeded 200 μm. To passage the tumor organoids, they were separated from the Matrigel by dissociating them with collagenase/dispase solution (Sigma-Aldrich): 500 μl of the solution (1 $mg{\cdot}ml^{-1}$) was mixed with the culture medium at 1:1 ratio and delivered into the well plate. The Matrigel was physically disrupted by mild pipetting, and the plate that held the organoids were placed in an incubator for 30 min at 37 °C and 5% CO_2 to enzymatically dissociate the residue. The mixture of tumor organoids was centrifuged and resuspended with 1 ml of the trypsin/EDTA solution (Hyclone) to dissociate the tumor organoids. They were mildly pipetted for 6 min at room temperature (RT), then washed with culture medium supplemented with 10% FBS (Gibco). They were used at early passages (<P10) to avoid clonal selection during passaging.

2.3. Inkjet printer setup and bioink preparation

We used an IJP system (MicroFab Inc. TX, USA) equipped with an *x*-*y* stage and a *z*-axis moving nozzle. To maintain stable jet formation, an 80 μm nozzle was used with applied voltage of ±80 V

throughout the experiments. The printing system was sterilized using 70% alcohol and UV-C lamp for 30 min before printing. The adaptors and connecting parts were washed with the alcohol and deionized water before the bioinks were loaded into the reservoir.

Tumor organoids were treated with trypsin to dissociate. They were resuspended in culture medium and filtered through a 40 μm mesh-size cell strainer to avoid nozzle clogging by the partially dissociated fragments. The cell concentration was adjusted to 5×10^5 or 1×10^6 cell·ml^{-1} depending on the experimental purpose, and the cells were counted using a commercial cell counter (Countess II FL, Invitrogen, CA, USA).

2.4. Single cell printing of bladder tumor cells

To culture organoids derived from single cells, single-drop printing was conducted on ultralow adhesion treated 384-well plate. Each well was filled with 50 μl of conditioned medium, which was prepared by exposing them to the mature tumor organoids for 2 d. They were filtered through a 0.45 μm pore-size syringe filter and supplemented with 2% (v·v^{-1}) Matrigel. Inkjet printing was conducted at the cell concentration of 5×10^5 cell·ml^{-1}, and the frequency was set to 2 Hz, which gave the highest proportion of drops that contained one cell. Wells that contained single cells were marked 3 h after the printing process. They were cultured in the 384-well plate until the organoids reached an average size >300 μm. To gather enough cells for gene expression analysis, the organoids were manually disrupted by pipetting, then cultured in Matrigel for another 7 d.

2.5. RNA extraction from organoids and cDNA synthesis

The organoids derived from single cells were treated with collagenase/dispase solution, then centrifuged to isolate tumor cells from extracellular mass. Total RNA was extracted from cell pellets by using an RNeasy Mini Kit (Qiagen, Germany), then quantified using NanoDrop® (Thermo Fisher Scientific). Samples with low RNA concentration (< 33 ng·μl^{-1}) were discarded to prevent errors in subsequent steps. RNA was reverse transcribed using a High Capacity cDNA Reverse Transcription Kit (Applied Biosystems, CA, USA) according to the manufacturer's instructions. Newly-synthesized cDNA was subjected to qRT-PCR.

2.6. Quantitative real-time PCR

Each cDNA reversely transcribed from mRNA was detected by qRT-PCR using a StepOnePlus Real-Time PCR System (Applied Biosystems) with SYBR Green master mix (Applied Biosystems). Forward and backward primer pairs (supplemental table S1 (available online at stacks.iop.org/BF/12/035030/mmedia)) were UPK1A, UPK2 and FOXA1 for human luminal-type tumor markers, and KRT5, KRT14 and KRT6A for human basal-type markers. The housekeeping gene, HPRT, was used to normalize the raw cycle threshold values as previously described [23]. After amplification steps, melting curves were generated to validate the PCR process. Every measurement was repeated three times.

2.7. Measuring viability and the tumor organoid growth kinetics

To measure the viability of the inkjet-printed cells, a printing nozzle was placed 1 mm above the surface of 500 μl of culture medium in a 2 ml vial. The cell concentration was set to 1×10^6 cell·ml^{-1}, and the cells were printed at 300 Hz with applied voltage of $\pm$80 V. The ink reservoir was gently pipetted every 10 min due to cell clogging and sedimentation during the process. The control group was maintained in the same cartridge vial during the printing process. The cells were stained using a live/dead assay kit (Invitrogen), and the viability was measured using the cell counter.

To measure the growth kinetics of the tumor organoids, tumor cells were overlain on the Matrigel substrate to allocate them on the same focal plane. First, 200 μl of Matrigel was spread on the wells of 24-well plate and solidified in the incubator for 15 min, then 1×10^5 tumor cells were added to each well with 2 ml of culture medium. Sizes were measured with the ImageJ software.

2.8. Analysis of cell number distribution in inkjet-printed droplets

Array patterns of 20 × 20 dots were printed on a glass substrate at cell concentrations of 5×10^5 or 1×10^6 cell·ml^{-1} to analyze the number of cell distribution within the droplets. The distance between dots was 500 μm and the stage velocity was set to 250 μm·s^{-1}, 500 μm·s^{-1}, or 1000 μm·s^{-1} to deliver cells at 0.5 Hz, 1 Hz, and 2 Hz respectively. Three sets of arrays were generated on each condition for statistical analysis, and the cell numbers were manually counted through an inverted microscope. The mean number of cells in each set was compared to the Poisson's distribution to measure the correlation of inkjet-printed cell pattern to the Poisson's distribution graph.

2.9. Immunohistochemistry

For immunohistochemistry, tumor organoids were fixed in 4% PFA for 20 min and embedded in OCT compound (Leica, Wetzlar, Germany). They were cut into 15–20 μm sections using Cryostat (Leica). Sections were dried overnight and post-fixed in 4% PFA for 20 min at RT. They were washed with PBS for three times and incubated with blocking buffer (5% goat serum and PBS containing 0.25% Triton X-100) for 1 h in RT. Primary antibodies were diluted with

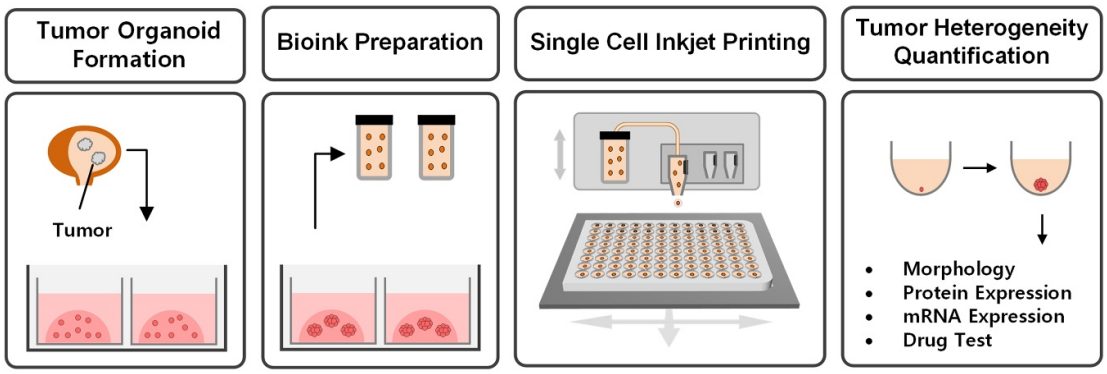

Figure 1. Quantifying bladder tumor hetergeneity by inkjet printing.

blocking buffer and applied to the samples for 4 h in RT: rat anti-CK-18 (DSHB, IW, USA), rabbit anti-Ki-67 (Abcam, UK), and rabbit anti-Caspase-3 (Cell signaling, MA, USA). The sections were then washed with PBS for three times, and incubated for 1 h at RT with secondary antibodies conjugated with Alexa Flour 488 or 594 (Invitrogen). Samples were washed with PBS for 3 times and treated with Hoechst 33342 (Invitrogen) for 5 min. After washing with PBS for 3 times, the sections were dried for 1 h in RT and mounted with Cytoseal XYL (Fisher Scientific, UK).

2.10. Drug treatment on tumor organoids

To compare the chemotherapeutic responses, single cell-derived tumor organoids were cultured for 14 d, and treated with cisplatin (Sigma-Aldrich) at 5 μM for 48 h. The drug containing culture medium was changed every 24 h. For the control group, same volume of PBS was added to the culture medium. The viability of the tumor organoids was measured based on the Caspase-3 expression.

3. Results

3.1. Concept of single cell printing process

The process of the assessment of intratumoral heterogeneity by inkjet printing consisted of four steps (figure 1). First, the tumor cells were acquired from bladder tumor patients and used throughout the research. They were 3D cultured into tumor organoid form in Matrigel to maintain the clonal heterogeneity of the parental tumor. After 8 to 10 d of culture, the tumor cells reached an average size of 150 μm. They were enzymatically dissociated into individual cell, and used as a bioink. The command script was written to deliver single droplets into each well of a ultralow adhesion treated 384-well plate. Following the printing process, wells that contained single cells were marked and observed to measure the growth kinetics. Heterogeneity was compared by measuring size, protein expression, drug responses, and mRNA expression of the single cell-derived tumor organoids.

3.2. Influence of inkjet printing process on the growth of tumor organoids

We observed the influence of inkjet printing on the tumor cells to validate the reliability of the process. The viability and growth kinetics were observed to measure the short-term and long-term influence respectively. The cells were printed into a 2 ml vial filled with 500 μl of culture medium, then their viability was measured immediately after the printing process. The viability of the printed group was slightly lower than the control group (83.2% and 88.6% respectively (figure 2(A)). However, it had negligible influence on the growth of the tumor organoids (figures 2(B) and (C)). The printed and non-printed tumor cells were overlain on Matrigel for clear comparison, and their size was measured every 2 d. Average sizes in the groups were similar throughout the growth until 6 d. These results show that inkjet printing is a safe method to assess ITH.

3.3. Optimization of printing procedure for efficiency of single-cell printing

To increase the efficiency of single cell delivery, we tested inkjet printing parameters that influence on the number of cells in the droplets. 20 $\times$ 20 dot arrays were printed on the glass substrate to allow analysis of the cell distribution patterns of the bladder tumor cells. Cells were printed at three ejection frequencies and relatively low cell concentrations (0.5×10^6, 1×10^6 cell·ml^{-1}) As can be seen figure 3 that the jet frequency influenced on the number of cells in the droplets. The average cell number was <1 at frequencies >2.0 Hz, while the number nearly doubled at 1.0 and 0.5 Hz respectively. Each pattern was in high correlation with Poisson's distribution (figures 3(A) and (B)); this result shows that the distribution can be adjusted without changing the ink concentration. The number of patient-derived tumor cells was limited, so we chose the condition with low ink concentration (5×10^5 cell·ml^{-1}) and set the frequency at 2.0 Hz, which provided the highest proportion of drops that contained single cells.

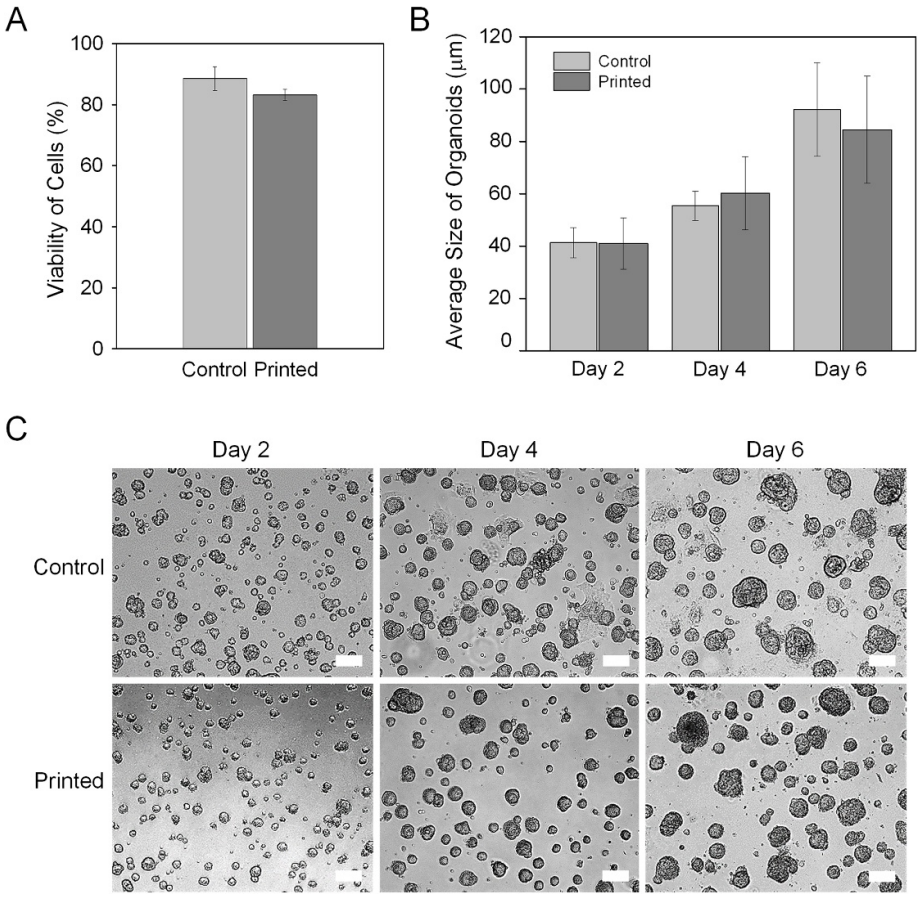

Figure 2. Influence of inkjet printing process on growth of tumor organoids. (A) Viability of tumor cells and (B) average size of tumor organoids of inkjet-printed and control groups. (C) Representative microscopic images of growth of tumor organoids of each group. Scale Bar: 100 μm.

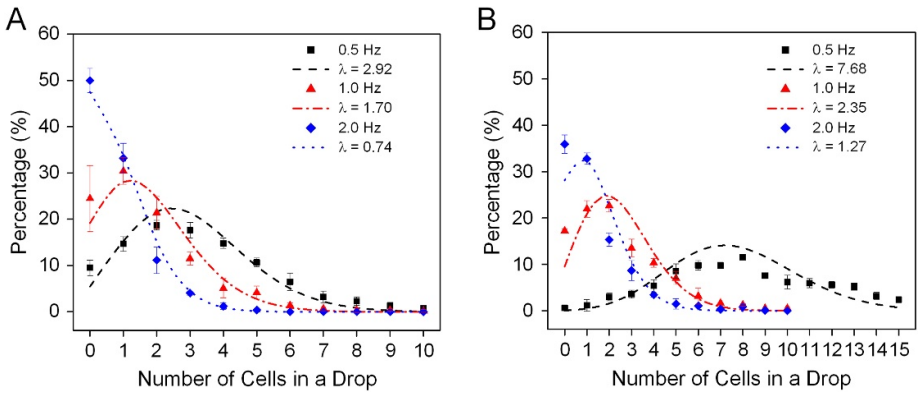

Figure 3. Printing parameter optimization. Distribution of numbers of cells in a printed drop with different cell concentrations: (A) 5×10^5; (B) 1×10^6 cell·ml^{-1}. Curves: correspoding Poisson's distribution with mean and variance λ.

3.4. Observation of various morphologies of single cell-derived tumor organoids

Next, we cultured the organoids that had been derived from single tumor cells in separate culture condition to quantify the ITH. Inkjet drops were printed on ultralow adhesion treated 384–well plates with one drop per well. The cell concentration of the bioink was set to 5×10^5 cell·ml^{-1} and was printed at 2.0 Hz to maximize the proportion of samples that had single cells. Each well was observed 3 h after the printing process to sort and track the growth of the resulting organoids.

The organoids exhibited different morphologies in growth. (figure 4(A)). They were similar until day 4, but differences were observed from day 8. Their sizes largely varied ranging from 22 μm to 244 μm (figure 4(B)), and the a few organoids showed disruptive morphologies (figure 4(A)(iv)). Immunohistochemistry analysis was performed to compare the expression of proteins related with proliferation

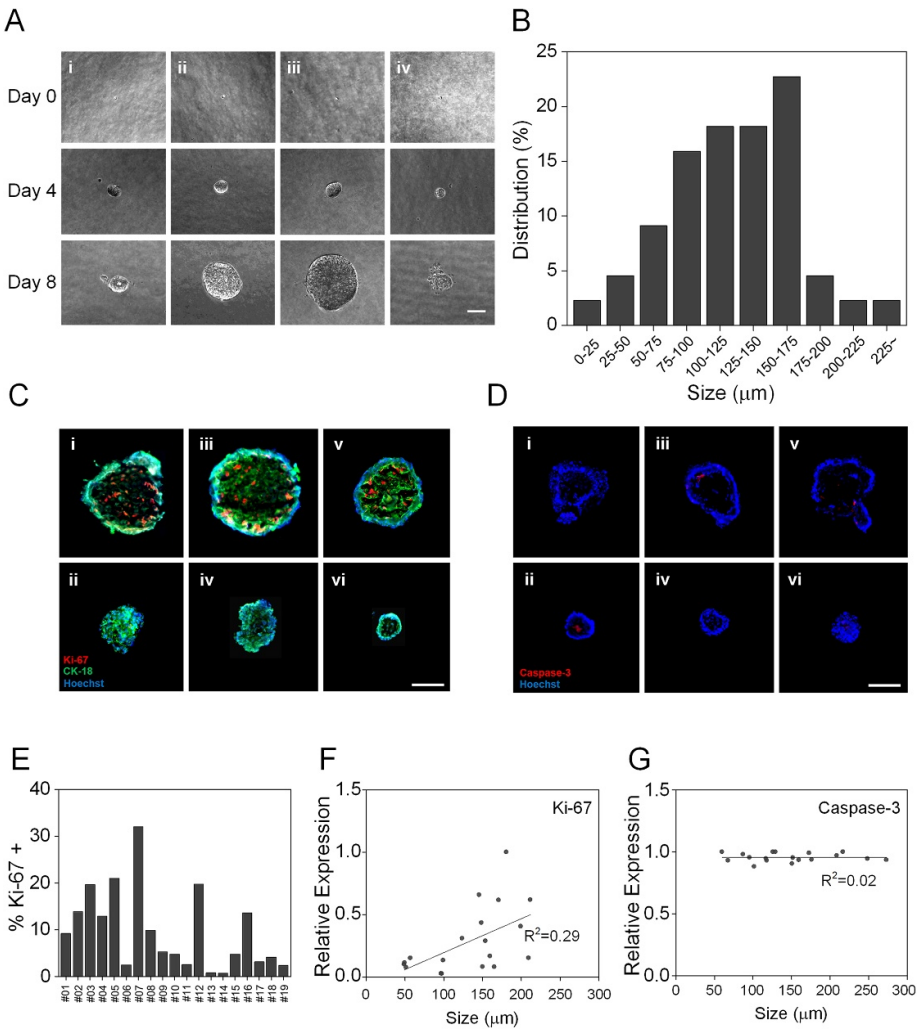

Figure 4. Morphologies and protein expressions of single cell-derived tumor organoids. (A) Representative microscopic images and (B) the distribution of different growth of single cell-derived tumor organoids. (C), (D) Immunofluorescent images of tumor organoids expressing CK-18, Ki-67, and Caspase-3. (E) Comparison of Ki-67 expression levels among the tumor organoids. (F), (G) Measuring correlation of size and relative protein expression of Ki-67 and Caspase-3. Scale bars: 50 μm.

and apoptosis, Ki-67 (figures 4(C), (E) and (F)) and Caspase-3 (figures 4(F) and (G)) respectively. The expression of Ki-67 was heterogenous among the tumor organoids (figure 4(E)), which was slightly correlated with the organoid sizes (figure 4(F)). However, the expression of Caspase-3 were homogeneous regardless of the size variances (figure 4(F)). We speculate that these variations are a result of different mutation profiles among the single cells that spawned the organoids.

3.5. Cisplatin treatment on single cell-derived tumor organoids

We applied chemotherapeutic drugs on the tumor organoids to observe whether the single cell-derived tumor organoids have heterogeneous drug responses (figure 5). After treatment of conventional chemotherapeutic drug, cisplatin, the expression of Caspase-3 was observed from 20 organoids. Cisplatin treatment induced lethal response from the tumor organoids (figures 5(A) and (B)). Compared to the control group, the mean viability decreased from 97.5% to 83.8% (figure 5(C)). Heterogeneous expression of Caspase-3 was observed from the cisplatin treated tumor organoids, ranging from 2.7% to 35.8% (figure 5(D)). Drug resistance was observed from a few organoids with smaller diameters (#12 and #18), but the statistical correlation was not observed between size and Caspase-3 expression (data not included).

3.6. Expression of luminal-type genes in single cell-derived organoids

To investigate the heterogeneity between the organoids derived from single cells, we measured relative gene expressions and compared them at a transcriptome level. First, the cells in the organoids were obtained from a patient who had a luminal-type tumor, so we measured representative mRNA levels with markers of luminal-type tumors (figures 6 and S1). Although the organoids were originated from cells in the same tissue, uroplakin-1a(UPK1A) mRNA expressions were distinctly expressed (figure 6(A)). For instance, UPK1A was expressed approximately

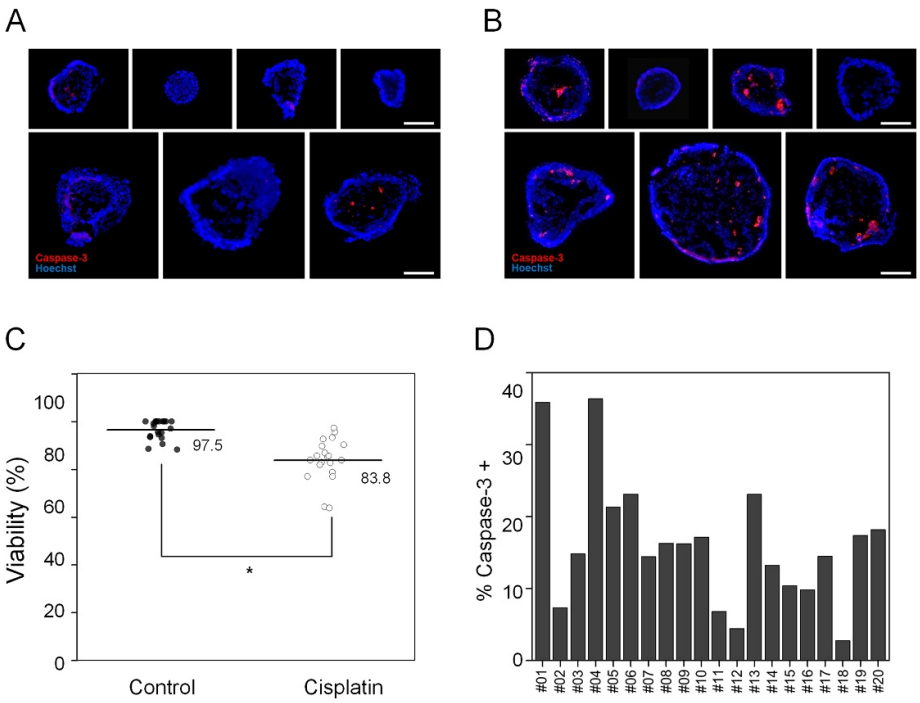

Figure 5. Responses of single cell-derived tumor organoids against cisplatin. Immunofluorescent images of tumor organoids after treatment of (A) PBS and (B) 5 μm of cisplatin. (C) Mean comparison of viability between the groups (n = 20, *p < 0.05). (D) Comparison of Caspase-3 expression levels among the tumor organoids.

four times higher in organoid #L27 than in organoid #L16 (figure S2). Different expression was also observed for uroplakin-2(UPK2). We also found differential expressions of UPK2 mRNAs in the organoids (figure 6(B)). We additionally examined expression of another gene, forkhead box protein A1(FOXA1). FOXA1 was highly expressed universally in the organoids, but the individual expression levels varied (figure 6(C)). This trend was shown repeatedly in the organoids derived from a patient who had a basal-type tumor. UPK1A and UPK2 mRNAs were distinctly expressed over 20 single cell-derived organoids (figures 6(D) and (E)) and the expression of FOXA1 mRNA was dramatically varied between the organoids (figure 6(F)).

3.7. Expression of basal-type genes in single cell-derived organoids

We further studied basal-type gene expressions to investigate the heterogeneity in luminal-type organoids. Keratin 5 (KRT5, also known as cytokeratin 5) primer was used to detect a gene expression, and interestingly we found a distinct upregulation of this mRNA in one luminal-type organoid with heterogeneous expression profiles (figure 7(A)). We additionally analyzed the mRNA expression, of keratin 14 (KRT14, also known as cytokeratin 14). KRT14 expressions differed among the organoids (figure 7(B)). We also examined with the keratin 6A (KRT6A). The level of KRT6A mRNA varied 1 to 4 times among the organoid samples (figure 7(C)). Moreover, we found that these 3 basal-type mRNAs were highly expressed in basal-type organoids (figure S3), and also observed heterogeneous expression of these mRNAs among the individual organoids.

4. Discussion

Intratumoral heterogeneity research requires single–cell approaches because the tumor tissue consists of multiple clones. In this study, we demonstrate that high-resolution, drop-on-demand IJP can be effectively used to assess ITH for the first time. As a non-contact, direct-write method, IJP offers unique capabilities and advantages to sort viable cells into microwell plates. Our results show that IJP can be performed in normal cell culture medium without the need for buffer solutions or for tagging the cells with dyes or antibodies. In addition, the influences of printing process on cell viability and growth of tumor organoid are negligible. The use of a motorized printing system and a design software allows living cells to be accurately allocated into predestined positions in a microwell plate, which can be further utilized to generate preclinical tumor models.

To demonstrate that inkjet printing is an effective tool to quantify ITH, we aimed to examine the heterogeneity of bladder tumor, which is complicated by its underlying genetic diversity. Bladder cancer is a highly prevalent disease that causes more than 190 000 deaths every year worldwide [24]. The multilayered bladder epithelium comprises a luminal layer of fully differentiated umbrella cells and a basal layer of Sonic Hedgehog positive cells [25, 26]. The Cancer Genome Atlas project introduced genomic

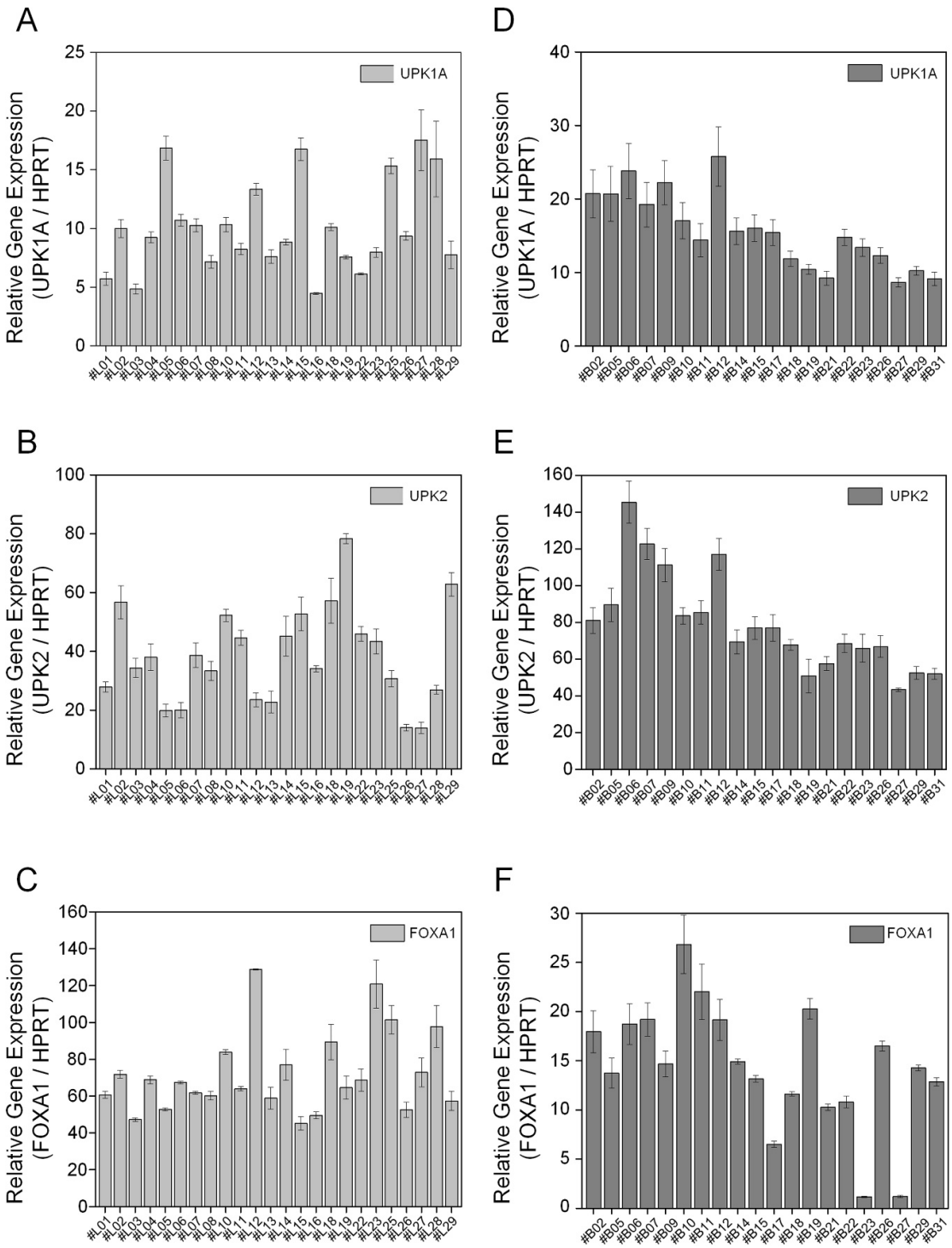

Figure 6. Gene expression profiles of luminal-type markers in both luminal- and basal-type tumor organoids. mRNA levels of luminal-type marker (A) UPK1A, (B) UPK2 and (C) FOX1A in 24 single cell-derived organoids from luminal-type tumor patient and (D) UPK1A, (E) UPK2 and (F) FOX1A in 20 single cell-derived organoids from basal-type tumor patient. Every expression level was normalized by the level of HPRT gene. The RNAs were not detected in some organoids.

taxonomy of basal and luminal molecular subtypes in muscle-invasive bladder cancer. There is an urgent need for more precise and efficient approach to classify the heterogeneity of bladder cancer [27].

In this study, we acquired tumor cells from the two types of bladder tumor patients and maintained them as organoids. Patient-derived organoids are known to recapitulate the histopathological and molecular diversity of human bladder cancer. Notably, they retain parental tumor heterogeneity [28, 29]. Variation was observed in the size of printed organoids, which was positively correlated with the Ki-67 expression level. Heterogeneity was also observed in their responses against cisplatin, where the Caspase-3 expression level varied from 2.7% to 35.8% with a few organoids showing drug resistance. When compared in mRNA level of the 44 organoids, we observed considerable variation in the mRNA

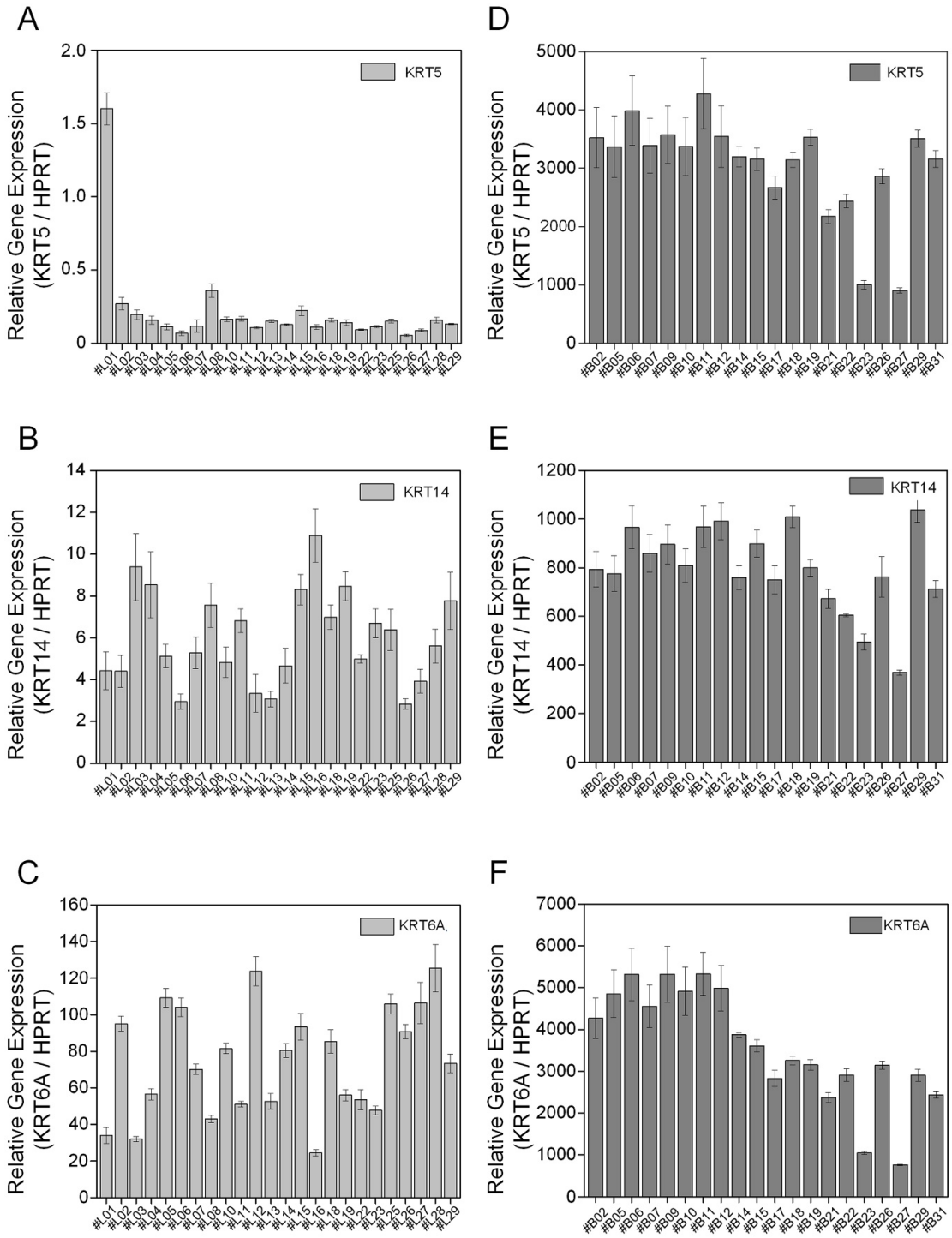

Figure 7. Gene expression profiles of basal-type markers in both luminal- and basal-type tumor organoids. mRNA levels of luminal-type marker (A) KRT5, (B) KRT14 and (C) KRT6A in 24 single cell-derived organoids from luminal-type tumor patient and (D) KRT5, (E) KRT14 and (F) KRT6A in 20 single cell-derived organoids from basal-type tumor patient. Every expression level was normalized by the level of HPRT gene. The RNAs were not detected in some organoids.

expression level of three representative luminal-type markers: UPK1A in bladder epithelium is a clear marker in luminal-type tumor [30, 31]; UPK2 is expressed in carcinomas and affects epithelial differentiation [32]; FOXA1 is involved in prognostic significances in cancer [33]. The same trend was observed with basal-type markers, a well-known basal epithelial marker KRT5 [34], KRT14 which is a type-I keratin that forms a heterodimer with keratin 5 [35, 36] and another type II keratin KRT6A [37]. Interestingly, after normalizing the expression level of each gene by the maximum value, we found a case of similar expression profile between #B23 and #B27 (figure S4), however, in the other cases the distinct expression tendency was remarkably observed (figures S2 and S4).

5. Conclusion

For the first time, we applied drop-on-demand inkjet process to assess genomic heterogeneity in human bladder tumor cells. We showed that direct inkjet printing of tumor cells in culture medium enabled efficient cell sorting into a microwell plate with any additive or additional treatment. We observed the negligible influence of printing process on the tumor cells. The cell concentration and jet frequencies were optimized to maximize the yield of single cell delivery. Single cells were cultured to induce organoid formation; their growth patterns were variable. This heterogeneity was measured by comparing the size and gene expressions on protein and mRNA level. Variations were observed on Ki-67, which was correlated with the size, and on Caspase-3 with a few organoids showing drug resistance when treated with cisplatin. More than forty organoids from both luminal- and basal-type tumor patients were acquired, and their differential gene expressions of luminal- and basal-type markers were quantified. Finally, the heterogeneity was widely observed. The results show the capability of inkjet to analyze tumor heterogeneity. Any types of cell can be inkjet-printed with optimized parameters. High-speed cell-sorting with high-throughput next-generation sequencing technologies could be of clinical benefit in the age of personalized medicine, uncovering more scientific details about ITH.

Acknowledgments

This work was supported by the National Research Foundation of Korea (NRF) grant funded by the Korea government (MSIT) (NRF-2018R1A2A3075391, NRF-2016M1A5A1027599) and by Gyeongbuk Science and Technology Promotion Center of Korea (SF317001A).

ORCID iD

Sungjune Jung https://orcid.org/0000-0001-9258-0572

References

[1] Alizadeh A A *et al* 2015 Toward understanding and exploiting tumor heterogeneity *Nat. Med.* **21** 846–53
[2] Jamal-Hanjani M, Quezada S A, Larkin J and Swanton C 2015 Translational implications of tumor heterogeneity *Clin. Cancer Res.* **21** 1258–66
[3] Lee J-K *et al* 2017 Spatiotemporal genomic architecture informs precision oncology in glioblastoma *Nat. Genet.* **49** 594–9
[4] Gagan J and Van Allen E M 2015 Next-generation sequencing to guide cancer therapy *Genome Med.* **7** 80
[5] Hu P, Zhang W, Xin H and Deng G 2016 Single cell isolation and analysis *Front. Cell Dev. Biol.* **4** 1–12
[6] Meyer M *et al* 2015 Single cell-derived clonal analysis of human glioblastoma links functional and genomic heterogeneity *Proc. Natl. Acad. Sci.* **112** 851–6
[7] Dimov I K, Lu R, Lee E P, Seita J, Sahoo D, Park S M, Weissman I L and Lee L P 2014 Discriminating cellular heterogeneity using microwell-based RNA cytometry *Nat. Commun.* **5** 1–12
[8] Park J Y, Morgan M, Sachs A N, Samorezov J, Teller R, Shen Y, Pienta K J and Takayama S 2010 Single cell trapping in larger microwells capable of supporting cell spreading and proliferation *Microfluid. Nanofluid.* **8** 263–8
[9] Klein A M, Mazutis L, Akartuna I, Tallapragada N, Veres A, Li V, Peshkin L, Weitz D A and Kirschner M W 2015 Droplet barcoding for single-cell transcriptomics applied to embryonic stem cells *Cell* **161** 1187–201
[10] Pellegrino M *et al* 2018 High-throughput single-cell DNA sequencing of acute myeloid leukemia tumors with droplet microfluidics *Genome Res.* **28** 1345–52
[11] Liu Y, Yang Q, Cao L and Xu F 2019 Analysis of leukocyte behaviors on microfluidic chips *Adv. Healthc. Mater.* **8** 1801406
[12] Wijshoff H 2010 The dynamics of the piezo inkjet printhead operation *Phys. Rep.* **491** 77–177
[13] Kim Y K, Park J A, Yoon W H, Kim J and Jung S 2016 Drop-on-demand inkjet-based cell printing with 30-μm nozzle diameter for cell-level accuracy *Biomicrofluidics* **10** 064110
[14] The R, Yamaguchi S, Ueno A, Akiyama Y and Morishima K 2013 Piezoelectric inkjet-based one cell per one droplet automatic printing by image processing *2013 IEEE/RSJ Int. Conf. on Intelligent Robots and Systems* pp 502–7
[15] Park T-M, Kang D, Jang I, Yun W-S, Shim J-H, Jeong Y, Kwak J-Y, Yoon S and Jin S 2017 Fabrication of in vitro cancer microtissue array on fibroblast-layered nanofibrous membrane by inkjet printing *Int. J. Mol. Sci.* **18** 2348
[16] Yoon S, Park J A, Lee H-R, Yoon W H, Hwang D S and Jung S 2018 Inkjet–spray hybrid printing for 3D freeform fabrication of multilayered hydrogel structures *Adv. Healthc. Mater.* **7** 1800050
[17] Park J A, Yoon S, Kwon J, Now H, Kim Y K, Kim W-J, Yoo J-Y and Jung S 2017 Freeform micropatterning of living cells into cell culture medium using direct inkjet printing *Sci. Rep.* **7** 14610
[18] Park J A, Lee H, Park S and Jung S 2020 Self-organization of fibroblast-laden 3D collagen microstructures from inkjet-printed cell patterns *Adv. Biosys.* **4**
[19] Xu T, Jin J, Gregory C, Hickman J J and Boland T 2005 Inkjet printing of viable mammalian cells *Biomaterials* **26** 93–99
[20] Xu T, Gregory C A, Molnar P, Cui X, Jalota S, Bhaduri S B and Boland T 2006 Viability and electrophysiology of neural cell structures generated by the inkjet printing method *Biomaterials* **27** 3580–8
[21] Gao B, Yang Q, Zhao X, Jin G, Ma Y and Xu F 2016 4D bioprinting for biomedical applications *Trends Biotechnol.* **34** 746–56
[22] Ji Y, Yang Q, Huang G, Shen M, Jian Z, Thoraval M-J, Lian Q, Zhang X and Xu F 2019 Improved resolution and fidelity of droplet-based bioprinting by upward ejection *ACS Biomater. Sci. Eng.* **5** 4112–21
[23] Shin K, Lim A, Zhao C, Sahoo D, Pan Y, Spiekerkoetter E, Liao J C and Beachy P A 2014 Hedgehog signaling restrains bladder cancer progression by eliciting stromal production of urothelial differentiation factors *Cancer Cell* **26** 521–33
[24] Bray F, Ferlay J, Soerjomataram I, Siegel R L, Torre L A and Jemal A 2018 Global cancer statistics 2018: GLOBOCAN estimates of incidence and mortality worldwide for 36 cancers in 185 countries *CA: Cancer J. Clin.* **68** 394–424
[25] Nedjadi T, Salem N, Khayyat D, Al-Sayyad A, Al-Ammari A and Al-Maghrabi J 2019 Sonic Hedgehog expression is associated with lymph node invasion in urothelial bladder *Cancer Pathol. Oncol. Res.* **25** 1067–73
[26] Kim S *et al* 2019 Epigenetic regulation of mammalian Hedgehog signaling to the stroma determines the molecular subtype of bladder cancer *Elife* **8** e43024

[27] Choi W et al 2014 Identification of distinct basal and luminal subtypes of muscle-invasive bladder cancer with different sensitivities to frontline chemotherapy *Cancer Cell* **25** 152–65
[28] Lee S H et al 2018 Tumor evolution and drug response in patient-derived organoid models of bladder cancer *Cell* **173** 515–528
[29] Drost J and Clevers H 2018 Organoids in cancer research *Nat. Rev. Cancer* **18** 407–18
[30] Lobban E D, Smith B A, Hall G D, Harnden P, Roberts P, Selby P J, Trejdosiewicz L K and Southgate J 1998 Uroplakin gene expression by normal and neoplastic human urothelium *Am. J. Pathol.* **153** 1957–67
[31] Robertson A G et al 2017 Comprehensive molecular characterization of muscle-invasive bladder cancer *Cell* **171** 540–556.e25
[32] Wu R-L, Osman I, Wu X-R, Lu M-L, Zhang Z-F, Liang F-X, Hamza R, Scher H, Cordon-Cardo C and Sun -T-T 1998 Uroplakin II gene is expressed in transitional cell carcinoma but not in bilharzial bladder squamous cell carcinoma: alternative pathways of bladder epithelial differentiation and tumor formation *J. Urol.* **160** 1937
[33] Warrick J I et al 2016 FOXA1, GATA3 and PPAR cooperate to drive luminal subtype in bladder cancer: a molecular analysis of established human cell lines *Sci. Rep.* **6** 38531
[34] Eckstein M et al 2018 mRNA-expression of KRT5 and KRT20 defines distinct prognostic subgroups of muscle-invasive urothelial bladder cancer correlating with histological variants *Int. J. Mol. Sci.* **19** 3396
[35] Alam H, Sehgal L, Kundu S T, Dalal S N and Vaidya M M 2011 Novel function of keratins 5 and 14 in proliferation and differentiation of stratified epithelial cells ed R D Goldman *Mol. Biol. Cell* **22** 4068–78
[36] Ramírez A, Bravo A, Jorcano J L and Vidal M 1994 Sequences 5′ of the bovine keratin 5 gene direct tissue- and cell-type-specific expression of a lacZ gene in the adult and during development *Differentiation* **58** 53–64
[37] Terada T 2013 Urinary bladder urothelial carcinoma with expression of KIT and PDGFRA and showing diverse differentiations into plasmacytoid, clear cell, acantholytic, nested, and spindle variants, and into adenocarcinoma, signet-ring cell carcinoma, small cell carcinom *Int. J. Clin. Exp. Pathol.* **6** 1150–6